Geophysical Research Letters

Supporting Information for

Hydrothermal fluids and where to find them: Using seismic attenuation an anisotropy to map fluids beneath Uturuncu volcano, Bolivia

T.S. Hudson[1], JM. Kendall[1], J.D. Blundy[1], M.E. Pritchard[2], P. MacQueen[2], S.S. Wei[3], J.H. Gottsmann[4], S. Lapins[4]

[1]Department of Earth Sciences, University of Oxford, UK

[2]Department of Earth and Atmospheric Sciences, Cornell University, USA

[3]Department of Earth and Environmental Sciences, Michigan State University, USA

[4]School of Earth Sciences, University of Bristol, UK

Contents of this file

Introduction

Here, we provide exact details of how the attenuation tomography and S-wave velocity anisotropy analysis was performed. We also include supplementary figures showing: the earthquake catalogue, tomography resolution tests, the magnetotelluric data from the literature, and additional seismic anisotropy results.

Supplementary Text 1: Attenuation tomography

Attenuation tomography comprises of using path-averaged attenuation observations, Q_{path}, between earthquake sources and receivers, to map the attenuation structure. The 3D attenuation tomography performed in this study is undertaken using the earthquakes and receivers shown in Figure 1, with the ray paths shown in Supplementary Figure S1. Our method is based upon that described in (Wei & Wiens, 2018) with some alterations, required due to the local nature of the study area. The critical observation we require to perform this inversion is the path-averaged attenuation, $\bar{Q}_{path}$, which is related to t*, given by,

$$t_i^* = \frac{t_i}{\bar{Q}_{path,i}} \quad ,$$

where t_i is the travel time of the seismic phase from the source to the receiver for earthquake ***i***. We obtain t*, and hence $\bar{Q}_{path}$, for each earthquake by calculating the displacement spectrum of the earthquake. We then assume that the source can be described by the Brune model (Brune, 1970), which is given by,

$$\Omega(f) = \frac{\Omega_0 e^{-\pi f t^*}}{\left(1 + \left(\frac{f}{f_c}\right)^2\right)} \quad ,$$

where ***f*** is the frequency, f_c is the corner frequency and Ω_0 is the long-period spectral amplitude. To find t*, we vary the parameters f_c, t*, and Ω_0 to find the Brune model that best matches the observed displacement spectrum for each earthquake source-receiver pair.

The observed t* values for all source-receiver pairs can then be used to perform a tomographic inversion to image the attenuation structure. The equation describing this tomography inversion is given by (Wei & Wiens, 2018),

$$t_i^* = \sum_{j=1}^{j=n_{nodes}} \frac{l_{ij}}{v_j}\frac{1}{Q_j} = G_{ij} m_j \quad ,$$

where n_{nodes} is the number of nodes in the 3D grid, l_{ij} is the path length for a ray associated with source-receiver pair i through node j, v_j is the seismic velocity of node j, Q_j is the quality factor measure of attenuation in node j, G_{ij} is the tomography tensor component associated with the source-receiver pair i and node j, and m_j is the tomography model attenuation for node j, where $m_j = \frac{1}{Q_j}$. The above equation can be rewritten in tensor notation as,

$$\boldsymbol{t}^* = \boldsymbol{G}.\boldsymbol{m} \quad ,$$

where $\boldsymbol{t}^*$ is a vector of length n_{pairs}, the number of source-receiver pairs, $\boldsymbol{G}$ is a second order tensor, and $\boldsymbol{m}$ is a vector of length n_{nodes}. We can solve this equation to find the model attenuation vector, $\boldsymbol{m}$, by performing a regularised linear least-squares inversion. This attenuation tomography method can be applied to P or S seismic phases to obtain Q_P or Q_S, respectively.

The above theory is implemented practically through the specific attenuation tomography steps as follows:

1. First we calculate the t_i^* measurements for each source-receiver pair to find $\boldsymbol{t}^*$. To do this we take a window around the P or S phase and compute the observed displacement spectrum using the multi-taper spectrum method of Krischer (2016) and Prieto et al. (2009). We then find the best-fitting Brune model to find the best estimates of $f_{c,i}$, t_i^*, and $\Omega_{0,i}$ for that source-receiver path. We repeat this for every source-receiver path to find $\boldsymbol{t}^*$. The Brune model does not always adequately fit the observed displacement spectrum. We filter out poor fits by removing source-receiver pairs associated with events that have a standard deviation in $\bar{Q}_{path}$, $\sigma_{\bar{Q}_{path}}$, greater than 400.

2. We then specify the 3D grid nodes for the tomographic inversion. We use a ***120 km*** by ***120 km*** by ***60 km*** grid with a uniform grid spacing of 1 km. We include the receivers inside the grid, with the adjacent nodes implicitly accommodating any local site effects in the tomographic inversion.
3. We then perform ray tracing to calculate the path lengths, l_{ij}, through each cell. We use the ray tracing code (Nasr et al., 2020), which uses the fast marching method (Lelièvre et al., 2011; Nicholas Rawlinson & Sambridge, 2005).
4. The final component we require to perform the tomographic inversion is the tomography tensor, **G**. This second order tensor is given by,
$$\boldsymbol{G} = \begin{pmatrix} \frac{l_{11}}{v_1} & \cdots & \frac{l_{1j}}{v_j} \\ \vdots & \ddots & \vdots \\ \frac{l_{i1}}{v_1} & \cdots & \frac{l_{ij}}{v_j} \end{pmatrix} .$$
5. We can then perform the regularised linear least squares inversion, which involves minimising the function,
$$f(\boldsymbol{m}) = \|\boldsymbol{Gm} - \boldsymbol{t}^*\|_2^2 + \lambda\|\boldsymbol{m}\| \quad ,$$
where λ is the regularisation coefficient. To find the optimal regularisation so as to avoid under- or over-fitting, we perform the inversion for multiple values of λ and select the value of λ at the corner of the L-curve. This provides us with the best fitting attenuation model ***m***.
6. The best fitting attenuation model may have physically unrealistic jumps in attenuation between individual cells. We account for this by applying smoothing to the model to produce a final, realistic attenuation model. There are various ways of applying smoothing to a tomography model. We apply 2D Gaussian smoothing over a wavelength of 1 km to each xy-plane layer in the 3D model. We apply lateral rather than vertical 2D smoothing since we are primarily interested in the attenuation variation with depth, and so do not want to introduce any unnecessary bias to the tomography result in this axis.

The steps to obtain t* measurements are implemented in the open source python code SeisSrcMoment (Hudson, 2020).

Supplementary Text 2: Seismic anisotropy

Seismic anisotropy in this study refers to S-wave velocity anisotropy. Such anisotropy can be broadly attributed to two factors: crystallographic orientation, where individual crystals of the medium preferentially align; and bulk-fabric anisotropy, typically caused by the preferential alignment of fractures that may be fluid-filled. Seismic anisotropy manifests itself as follows. An S-wave radiated from an earthquake source will have an initial polarisation. For a double-couple source, this polarisation is parallel to the slip-direction of the fault generating the earthquake. If a region of the crust is seismically anisotropic, then as the S-wave propagates through this region, the energy will be partitioned into two orthogonal components, one oriented in the plane of the fast-direction, ϕ, and the other in the plane of the slow-direction. Stronger anisotropy or a longer ray path through the anisotropic region will result in greater delay-times between these fast and slow S-waves . This phenomenon is called shear-wave splitting (Crampin, 1981; Silver & Chan, 1991). Shear-wave splitting is measured using SWSPy (Hudson, 2022), which is based on the eigenvalue method described in Teanby et al. (2004) and Walsh et al. (2013). The strength of anisotropy is quantified by the delay-time, δt. However, it is also useful to measure the strength of anisotropy, a, as the magnitude of splitting normalised by the distance travelled (Thomas & Kendall, 2002). If the delay time is defined by,

$$\delta t = t_{slow} - t_{fast} = \frac{d}{\bar{v}\left(1 - \frac{a}{2}\right)} - \frac{d}{\bar{v}\left(1 + \frac{a}{2}\right)} \quad ,$$

where d is the ray path length and $\bar{v}$ is the mean velocity of the medium, then the magnitude of anisotropy is given by (Thomas & Kendall, 2002),

$$a = \delta v_S = -\frac{2d}{\bar{v}\delta t} \pm \sqrt{\left(\frac{2d}{\bar{v}\delta t}\right)^2 + 4} \quad .$$

Supplementary figures

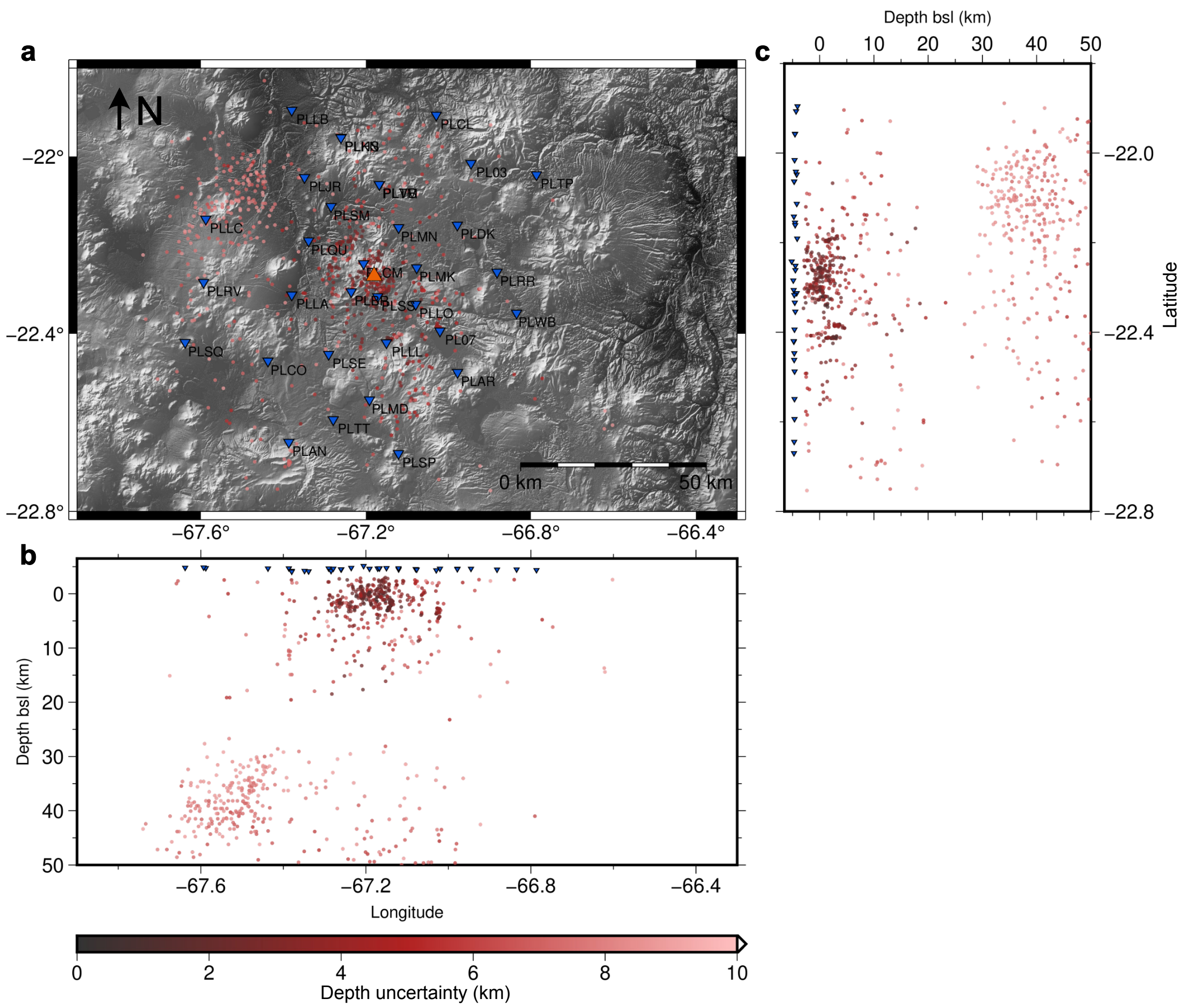

Supplementary Figure 1. Seismicity used in this study. Blue inverted triangles show seismometer locations. Red scatter points show earthquake hypocentres, coloured by uncertainty in depth.

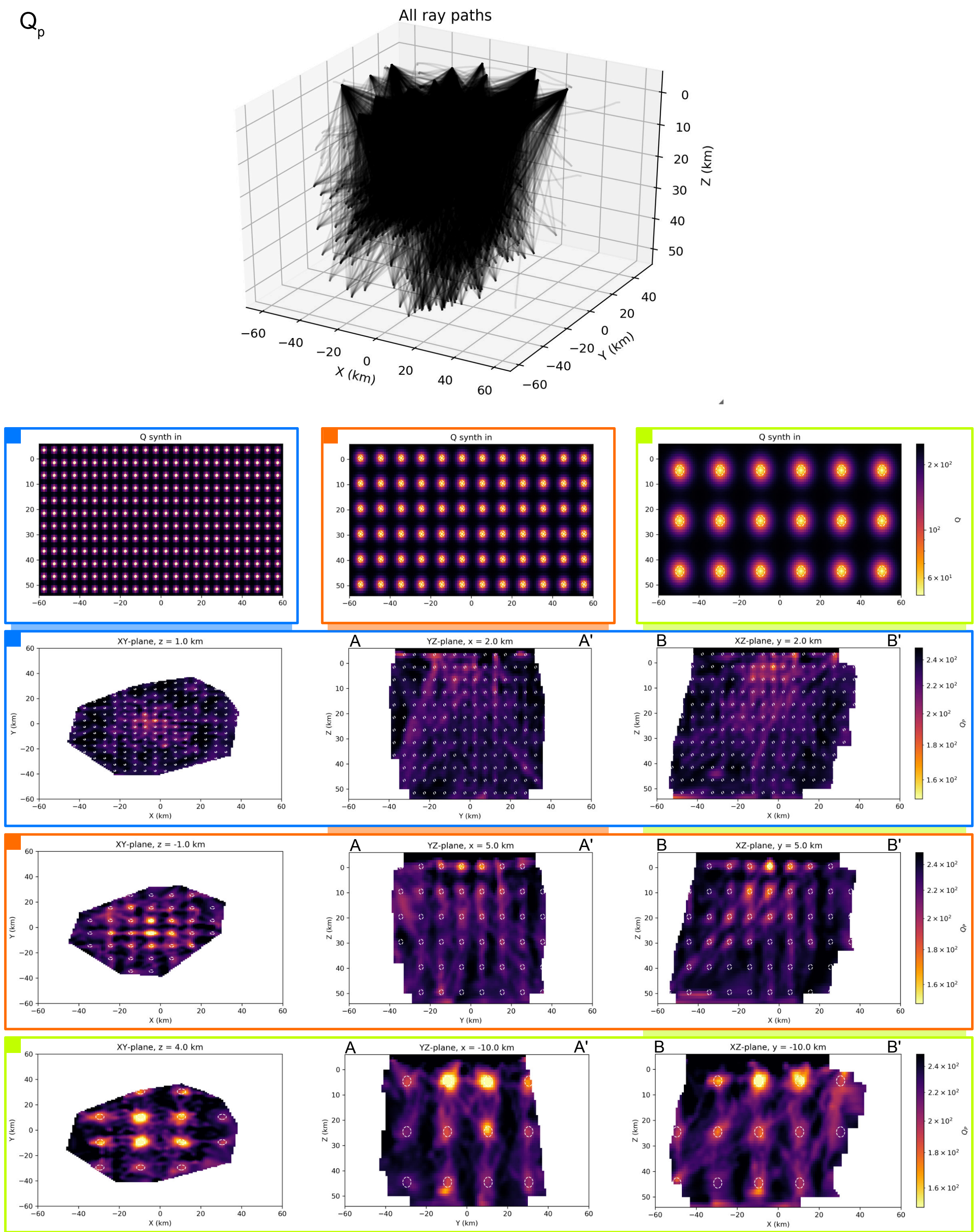

Supplementary Figure 2. Q_P tomography sensitivity analysis. Sensitivity analysis performed based on the theory in Rawlinson & Spakman (2016).

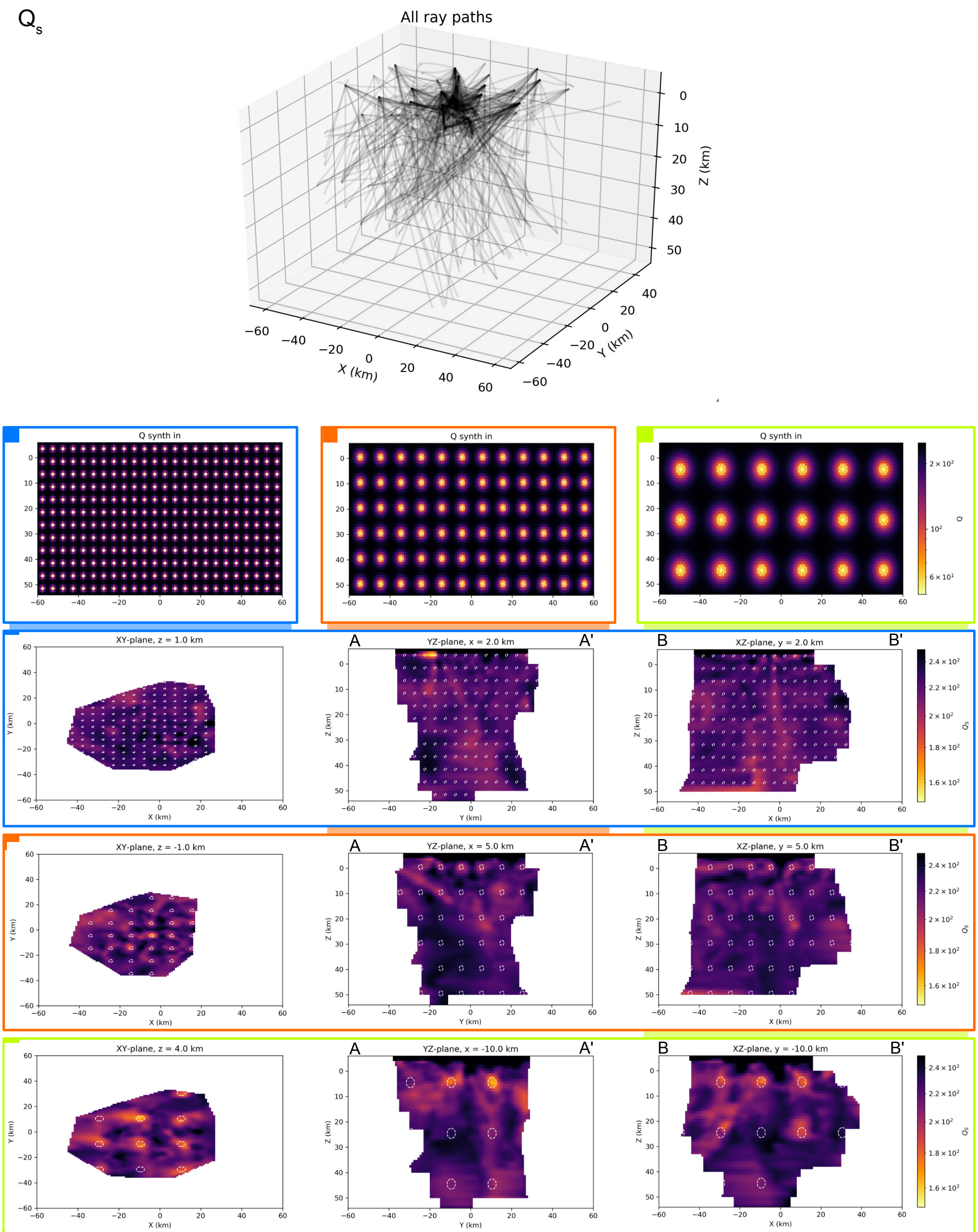

Supplementary Figure 3. Q_S tomography sensitivity analysis. Sensitivity analysis performed based on the theory in Rawlinson & Spakman (2016).

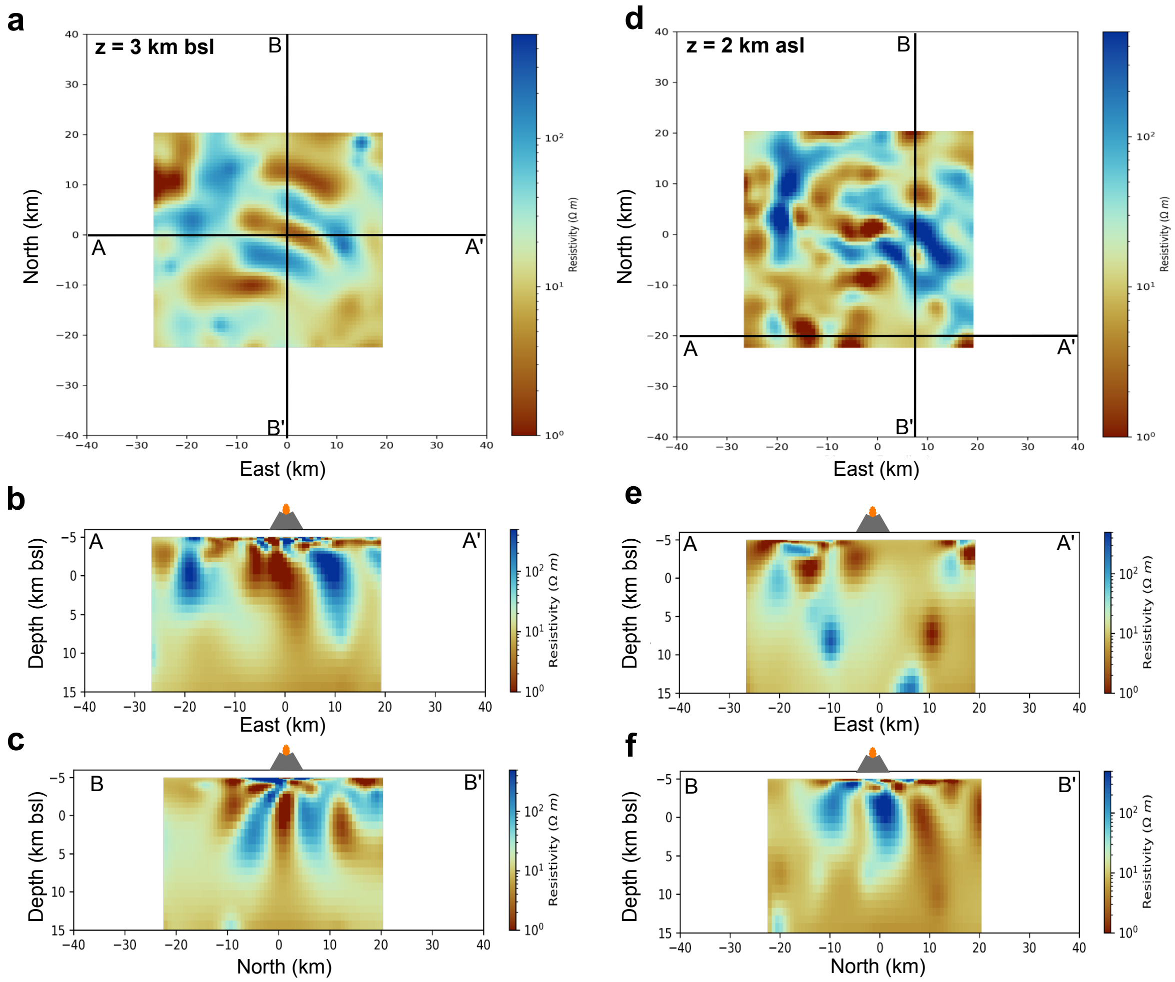

Supplementary Figure 4. Magnetotelluric tomography results from Comeau et al. (2016)**.**

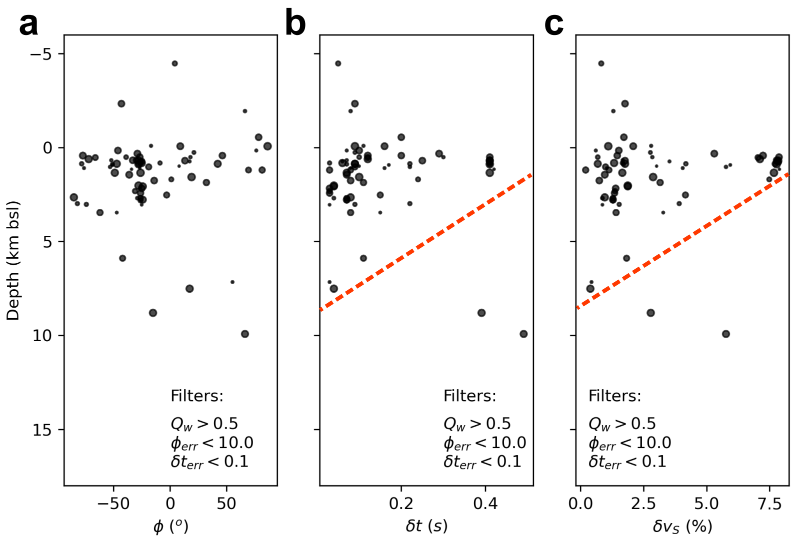

Supplementary Figure 5. Shear-wave velocity anisotropy with depth. (a), (b), (c) Fast directions, delay-times and fractional-change in S-wave velocity with depth, respectively. Relative sizes of scatter points are determined by their associated anisotropic quality factor, Q_W. Red dashed lines in (b), (c) indicate the approximate decreasing trend in delay-time and velocity-change with depth.